Rocky Worlds DDT: JWST Data Analysis Report for LTT 1445 A c

Misty Cracraft and Taylor J. Bell
JWST Data Analysis Team

October 21, 2026

1 Observation Overview

Under the RWDDT program, JWST-DDT-9234 Observation 1 obtained time-series imaging of LTT 1445 A c using MIRI/F1500W with the SUB64 subarray, covering 3.95 hours with the goal of measuring the secondary eclipse of the planet. This observation also unintentionally captured the transit of LTT 1445 A b which co-incided with the secondary eclipse of LTT 1445 A c. High Level Science Products (HLSPs) from this observation are hosted on MAST and include both intermediate and final results to help drive research-community engagement.

We measured both the centroid position and width of the target's point-spread function (PSF) during each integration. The telescope pointing remained quite stable along the x and y axes through the observation although with some high-frequency jitter seen along the y-axis, and the width of the PSF along both axes was also quite stable after an initial settling period of $\sim$30 minutes (see Figure 1).

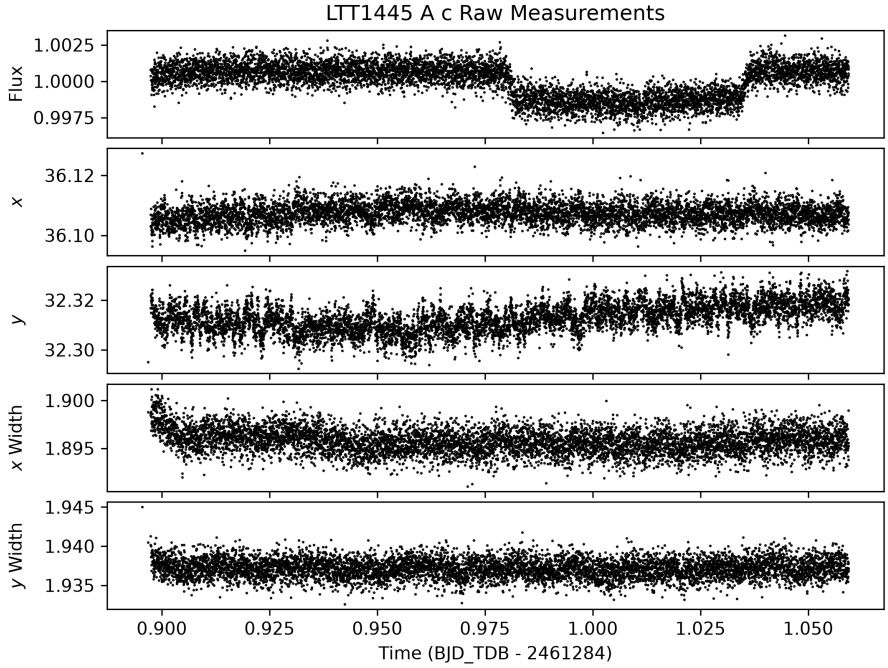

Figure 1: Stability of flux, centroid, and PSF. Time series of changes in the normalized raw flux, centroid position (x, y), and PSF width (computed as a Gaussian standard deviation along the x and y axes), illustrating initial settling behavior and overall pointing stability.

2 Data Reduction

This analysis used the standard JWST pipeline (`jwst` v2.0.1, with CRDS context file `jwst_1535.pmap`) for detector-level calibrations. Stage 1 processing included running the following steps: `emicorr`, `saturation`, `reset`, `linearity`, `rscd` (changed to skip the first 3 groups), and `jump` (with the threshold increased from 4.0 to 5.0). In Stage 2 we ran the `flat_field` step, but we disabled the `photom` step as flux-calibrated data are not desired for time-series analyses.

Photometric extraction and light curve fitting were completed using Stages 3–5 of the `Eureka!` Python package (1.5.dev230+g52cf7bef0). A time series was constructed for each pixel, and 5σ outliers (along with all `NaN` values) were replaced using bilinear interpolation over the nearest neighbors. Next, a center-of-mass centroid was calculated for each integration using `Eureka!`'s 'mgmc' method. The width of the target's PSF along the x and y axes were measured in each integration using a 2D Gaussian fit (see Figure 1) using pixels within 15 px of the centroid. These centroid and PSF-width measurements were compiled into co-trending vectors that were subsequently used as independent variables in the systematics modeling.

Photometric light curves were extracted in Stage 3 of `Eureka!` using the `photutils` package with circular apertures and 'exact' edges, where pixels are weighted by the fraction of their area lying within the specified aperture. A range of aperture and background annulus radii were considered. Aperture radii ranged from 5–9 pixels, in 1-pixel steps. The inner radius of the background annulus varied from 7 to 15 pixels in 2-pixel steps, while the annulus width ranged from 9 to 10 pixels in 1-pixel steps. Photometric light curves were generated for each source aperture + background annulus pair. In Stage 4, we chose to mask any integrations lying 6σ away from the rolling median using a boxcar filter with a width of 33 integrations.

3 Light Curve Fitting

During the initial analysis of the photometric light curve, we discovered that the dominant component of the light curve was a transit of LTT 1445 A b, while the predicted circular-orbit eclipse for LTT 1445 A c occurred in the middle of that transit. As such, we simultaneously fit our light curve with a `batman` transit model for LTT 1445 A b and a `batman` eclipse model for LTT 1445 A c in `Eureka!`'s Stage 5. The first 150 integrations were trimmed to remove the steepest part of the initial detector settling ramp, while simultaneously preserving a long enough pre-eclipse baseline to adequately sample the out-of-eclipse flux level. The remaining ramp-like feature was modeled using an exponential function in time.

Our full fitted model can be written as:

$$A(t) = F_*(t)\, E(t)\, S(t), \tag{1}$$

where $F_*(t)$ is the `batman` transit model of LTT 1445 A b, $E(t)$ is the `batman` eclipse model of LTT 1445 A c, and $S(t)$ describes the instrumental systematics and is given by

$$S(t) = P(t)\, R(t)\, X\big(x(t)\big)\, Y\big(y(t)\big)\, SX\big(sx(t)\big)\, SY\big(sy(t)\big), \tag{2}$$

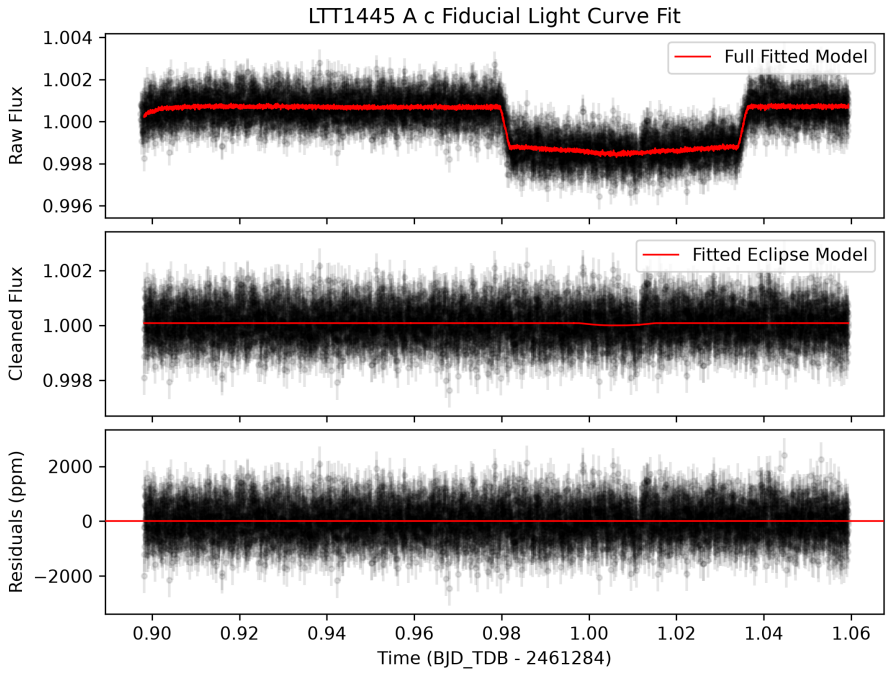

Figure 2: Fiducial light curve fit. *Top:* Raw, normalized flux measurements in black with the full systematics $\times$ astrophysical model over-plotted in red. The first 150 integrations were not included in the fit. *Middle:* Systematics-divided (and transit-removed) flux measurements are shown in black, with the eclipse model shown in red. *Bottom:* "Data $-$ model" residuals.

where

$$P(t) = c_0 + c_1(t - \bar{t}) \tag{3}$$

is a linear trend in time, and

$$R(t) = 1 + r_0 \exp\left[-r_1(t - t_{\rm start})\right] \tag{4}$$

models the detector settling exponential ramp. The centroid position and PSF width decorrelation terms are each assumed to be linear, for example,

$$X(x) = 1 + c_x(x - \bar{x}), \tag{5}$$

where $(x(t), y(t))$ is the measured centroid position as a function of time, $(sx(t), sy(t))$ is the PSF width along the x- and y-axes as a function of time, $(\overline{x}, \overline{y})$ is the time-averaged centroid position, and $(\overline{sx}, \overline{sy})$ is the time-averaged PSF size.

All model parameters were sampled simultaneously using the `dynesty` dynamic nested sampling algorithm. We used an initial 171 live points with the 'rwalk' sampling algorithm and the 'multi' bounds and an initial $d\log\mathcal{L} < 0.01$ stopping criterion. Subsequent batches of 85 live points were then iteratively added with `pfrac` set to 0.5 (balancing the improvement in the precision of the posterior and evidence) until the default stopping criterion was achieved. Our best-fit light curve model is shown in Figure 2, and the results of our fits are summarized in Table 1.

Table 1: The model priors for the fiducial fit. Fixed astrophysical parameters are shown without uncertainties and are taken from the juliet$_{\rm circ}$ fit from CIT's orbit fitting efforts during observational scheduling. Gaussian priors are shown as $\mathcal{N}(\mu, \sigma)$ with mean μ and standard deviation σ, while Uniform priors are shown as $\mathcal{U}(l, u)$ with lower-limit l and upper-limit u.

Parameter	Prior	Posterior
LTT-1445 A Parameters		
$R_*/R_\odot$ [†]	0.271	–
Quadratic Limb-Darkening Parameters		
u_1	$\mathcal{U}(-0.5, 2)$	$0.34^{+0.14}_{-0.15}$
u_2	$\mathcal{U}(-1, 2)$	$-0.26^{+0.21}_{-0.20}$
LTT-1445 A b Parameters		
P (days)	$\mathcal{N}(5.35876726, 0.00000059)$	$5.35876803^{+0.00000047}_{-0.00000043}$
t_0 (BMJD$_{\rm TDB}$)	$\mathcal{N}(60920.111737, 0.000020)$	$60920.111749^{+0.000019}_{-0.000018}$
b	$\mathcal{N}(0.170, 0.044)$	$0.166^{+0.030}_{-0.034}$
a/R_*	$\mathcal{N}(30.96, 0.26)$	$30.91^{+0.16}_{-0.17}$
e	0	–
$R_{\rm p}/R_*$	$\mathcal{N}(0.045, 0.020)$	$0.04459^{+0.00024}_{-0.00024}$
LTT-1445 A c Parameters		
P (days)	3.1238958612	–
$t_{\rm sec}$ (BMJD$_{\rm TDB}$)	$\mathcal{N}(58413.6452, 0.0015)$	$58413.6458^{+0.0011}_{-0.0011}$
b	0.9628928474	–
a/R_*	21.6059830937	–
e	0	–
$R_{\rm p}/R_*$	0.0385841722	–
$F_{\rm p}/F_*$ (ppm)	$\mathcal{N}(187, 500)$	83^{+56}_{-56}
Systematics Parameters		
c_0	$\mathcal{N}(0.999, 0.01)$	$1.000616^{+0.000056}_{-0.000056}$
c_1	$\mathcal{N}(0.0, 0.1)$	$0.00009^{+0.00022}_{-0.00022}$
r_0	$\mathcal{N}(0.00, 0.01)$	$-0.000535^{+0.000095}_{-0.000106}$
r_1	$\mathcal{U}(3, 1000)$	331^{+126}_{-86}
c_y	$\mathcal{N}(0, 0.5)$	$-0.0002^{+0.0016}_{-0.0015}$
c_x	$\mathcal{N}(0, 0.5)$	$-0.0066^{+0.0023}_{-0.0023}$
c_{sy}	$\mathcal{N}(0, 0.5)$	$0.0218^{+0.0060}_{-0.0059}$
c_{sx}	$\mathcal{N}(0, 0.5)$	$0.0287^{+0.0057}_{-0.0060}$
scatter_mult	$\mathcal{U}(0.8, 10)$	$1.1716^{+0.0092}_{-0.0094}$
Residual Std. Dev. (ppm)	—	$628.8^{+4.9}_{-5.1}$

[†]The stellar radius is used to account for the difference in light travel time throughout the planets' orbits.

3.1 Results & Discussion

During our analysis, we found that the inferred eclipse depth of LTT 1445 A cis dependent on the choice of time-of-eclipse priors. If we assume a close-to-circular orbit, we get 83 ± 56 ppm. If we instead allow for a more eccentric orbit, we find eclipse depths between 100 to 133 ppm with uncertainties of 40 to 53 ppm, depending on other priors used. We found that the time-of-eclipse is uncertain and/or degenerate with the limb-darkening coefficients. Allowing the sampler to explore non-physical quadratic limb-darkening coefficients results in a shift of mid-eclipse. Meanwhile, forcing physical LD coefficients (using the Kipping+2013 parameterization, which also biases the LD coefficients) results in time-of-eclipse posteriors that are consistent with our circular-orbit prediction, though with many modes in the posterior spanning a wide range.

An as-yet unexplained ∼+100 ppm jump at BMJD_TDB ≈ 61284.5120, preceded by a few minutes of slightly low flux, was seen in the data around the expected time of the eclipse of LTT 1445 A c (see Figure 3). An exploration was undertaken to attempt to determine the cause of this light curve feature with support from Claude's Opus 5.5 agentic-AI model as accessed through GitHub CoPilot. We have ruled out the following as possible causes for the jump: a) an HGA move (no HGA moves happened during these observations); b) pointing or psf changes (our linear decorrelation only fits for ∼2 ppm features, and no higher-order correlation is seen by-eye); c) mirror/tilt event or psf reshaping (the feature does not go away with larger apertures); d) cosmic rays (no major showers or suspect hits near the PSF core).

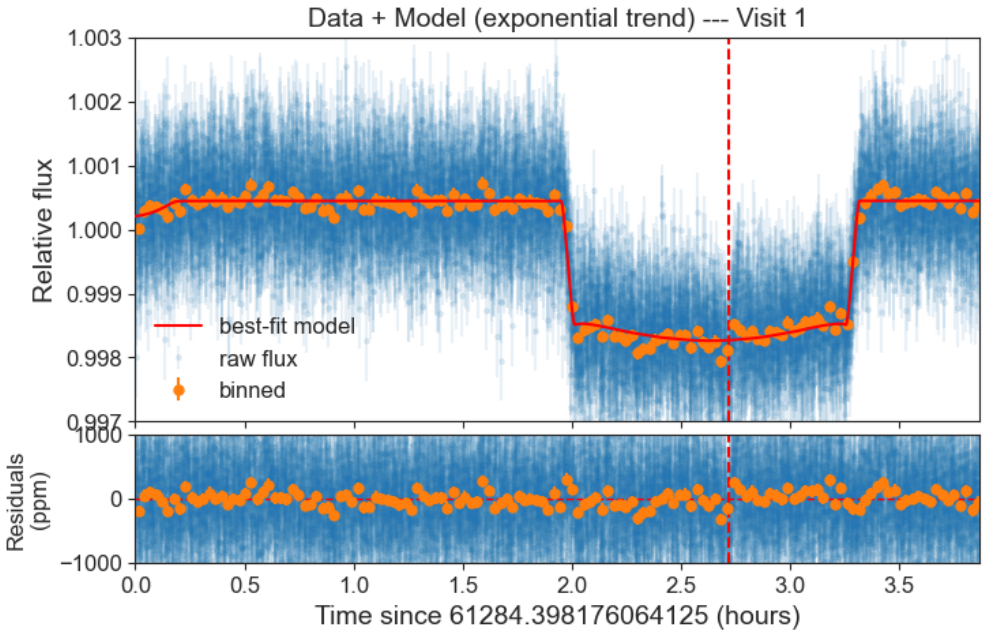

Figure 3: Unexplained jump in eclipse data. *Top:* The raw, normalized flux measurements in blue with the binned data in orange dots and the best fit model over-plotted in red. The vertical red dashed line highlights the unexplained jump. *Bottom:* The "data − model" residuals.

If we assume the light curve feature is part of the eclipse of LTT 1445 A c, then we can examine what this might tell us about the parameters of LTT 1445 A c. The amplitude matches LTT 1445 A c's expected 15 μm eclipse depth ($\sim$130 ppm for a bare rock), and the timing is close to the predicted eclipse, however a sharp step fits better than any explored eclipse shapes. If the feature comes from LTT 1445 A c, the eclipse must be less grazing than the transit geometry implies and it would also have to be centered $\sim$15 min earlier than circular-orbit predictions, all still consistent with the published $e < 0.22$.

4 Calibrated Stellar Flux Measurement

Following the methodology of Gordon et al. (2025), we measured absolutely-calibrated stellar photometry using `calints` FITS files with a 5.69 px aperture and an 8.63–11.45 px background annulus, applying an aperture correction of 1.497. Using the out-of-transit integrations spanning 0.03 days ($\sim$43 minutes) before and after the transit of planet b, we obtained a calibrated stellar flux of 71.05 ± 0.47 mJy.

5 Discussion and Outlook

This report presents the analysis of the first RWDDT JWST eclipse observation of LTT 1445 A c. With the transit of LTT 1445 A b overshadowing the eclipse signal, and with an unexpected jump in the time of the eclipse, analysis of this dataset was not trivial. Additional eclipse observations will be needed to better understand the eclipse depth of LTT 1445 A c. A combined fit of the other RWDDT observations of LTT 1445 A c and LTT 1445 A b should help determine if the jump seen in these data is astrophysical in origin.